Dirty limit scattering behind the decreased anisotropy of doped $YBa_2Cu_3O_{7-}$ thin films

2016 J. Phys.: Condens. Matter 28 175702

(http://iopscience.iop.org/0953-8984/28/17/175702)

IOP Publishing Journal of Physics: Condensed Matter
J. Phys.: Condens. Matter **28** (2016) 175702 (6pp) doi:10.1088/0953-8984/28/17/175702

Dirty limit scattering behind the decreased anisotropy of doped $YBa_2Cu_3O_{7-\delta}$ thin films

M Malmivirta[1,2], H Palonen[1], S Inkinen[3], L D Yao[3], J Tikkanen[1,2], H Huhtinen[1], R Jha[4], V P S Awana[4], S van Dijken[3] and P Paturi[1]

[1] Department of Physics and Astronomy, Wihuri Physical Laboratory, University of Turku, FI-20014 Turku, Finland
[2] University of Turku Graduate School (UTUGS), University of Turku, FI-20014 Turku, Finland
[3] Department of Applied Physics, NanoSpin, Aalto University School of Science, PO Box 15100, FI-00076 Aalto, Finland
[4] Superconductivity Division, National Physical Laboratory (CSIR), New Delhi 110012, India

E-mail: mika.malmivirta@utu.fi

Received 22 December 2015, revised 29 February 2016
Accepted for publication 10 March 2016
Published 5 April 2016

Abstract

We measured the resistivity of pulsed-laser-deposited $BaCeO_3$ (BCO)-doped YBCO thin films containing spherical BCO particles in fields up to 30 T. The average diameter of the particles depends on the dopant concentration being below 4 nm in all the samples. Raised values of the upper critical field, B_{c2}, were observed in all the samples. Additionally, the parameter γ, describing the electron mass anisotropy, decreased from 6.2 in the undoped sample to 3.1 in the 8 wt.% BCO-doped sample. These results can be explained by the increased number of defects decreasing the mean free path of electrons and thus lowering the coherence length, which in turn increases B_{c2}.

Keywords: anisotropy, artificial pinning centers, critical fields, pulsed-laser deposition, YBCO

(Some figures may appear in colour only in the online journal)

1. Introduction

The performance of high-temperature superconductors in high magnetic fields is crucial for future applications. One very commonly used procedure for improving the performance of YBCO thin films for applications in magnetic fields is to add non-superconducting dopants to the YBCO matrix. The improvement achieved by adding a dopant is quantified by measuring the relevant critical quantities, some of which are extrinsic, like the critical current density J_c, and others intrinsic, like the upper critical field B_{c2}.

It is preferred for the dopant not to react chemically with the YBCO, meaning the intrinsic properties of the YBCO should not change. However, an increase of B_{c2} has been seen [1, 2] when measuring $BaZrO_3$ (BZO)-doped YBCO. According to these results, the change occurs both in pulsed-laser-deposited (PLD) films and chemical-solution-deposited (CSD) films. In PLD-made films, BZO forms columnar, correlated structures [3, 4] with diameters below 10 nm [4, 5], somewhat larger than the sizes of the vortex cores at low temperatures. In contrast, if films are made by CSD, BZO forms much larger, non-correlated, mostly randomly oriented particles with a diameter of 30 nm [2, 6]. Based on these arguments, the increase of B_{c2} is unlikely to be caused by a certain size or shape of dopant particle. Additionally, small (a couple of nanometers in diameter [7]), topotaxially grown spherical particles are formed as $BaCeO_3$ (BCO)-doped YBCO is deposited using PLD.

In applications, YBCO is used as a coated conductor, i.e. deposited on a buffered thin metal tape. Also, the weakest direction of a superconductor determines its feasibility in applications in a magnetic field and thus the smaller the anisotropy is, the better. In addition to improving the magnetic field dependence of J_c, the other aim of doping from the coated conductors' point of view is to make the anisotropy of YBCO smaller for magnetic field applications. Anisotropy can be described using the Blatter scaling [8], which is usually applied to B_{c2} as

$$B_{c2}(\theta) = B_0\left(\frac{\sin^2(\theta)}{\gamma^2} + \cos^2(\theta)\right)^{-1/2}, \qquad (1)$$

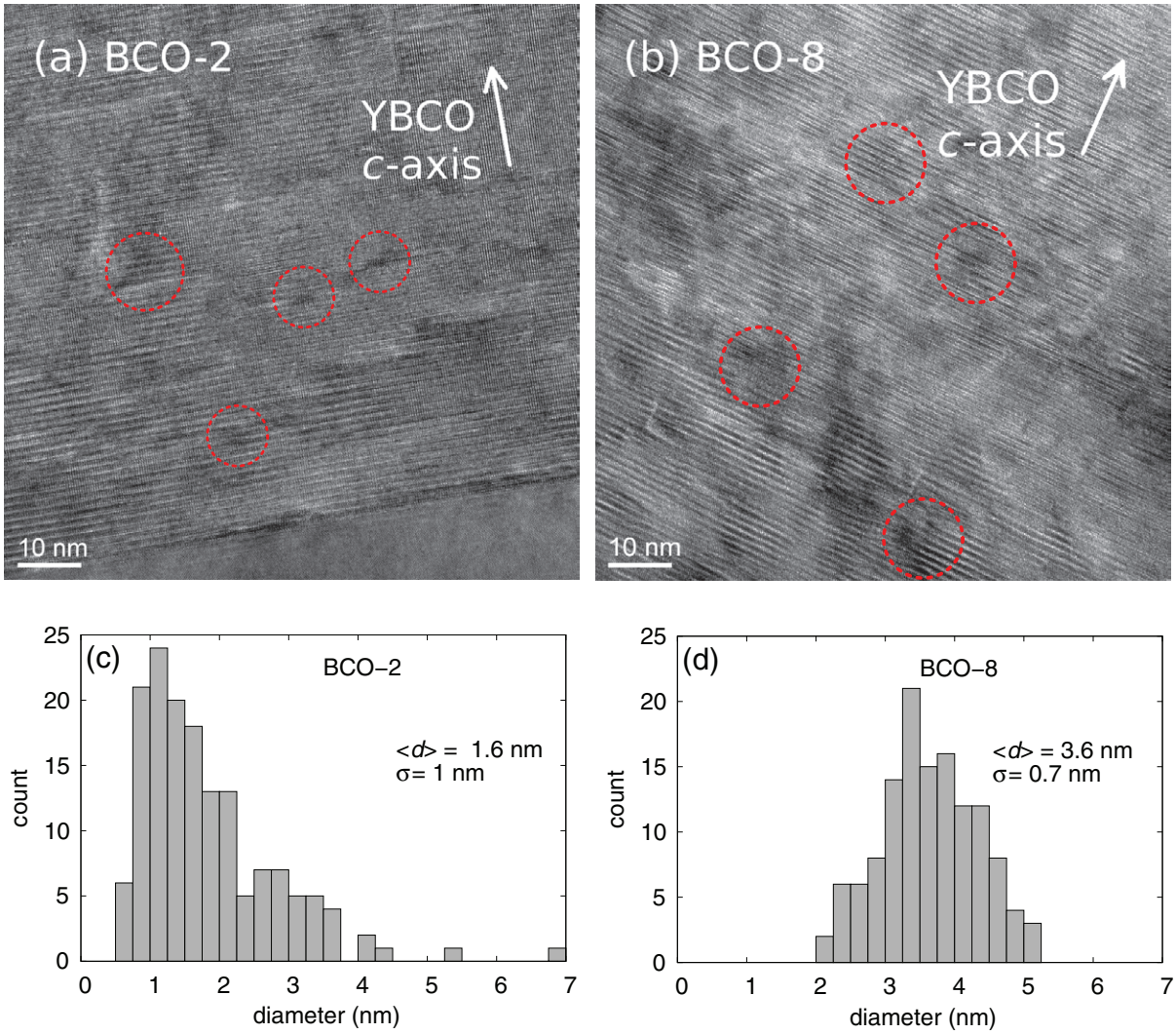

Figure 1. (a)–(b) The cross sectional TEM image of BCO-2 and BCO-8. The dotted line circles show some of the BCO particles. (c)–(d) The size distributions of the BCO particles in the samples. The averages, $\langle d \rangle$, and the standard deviations, σ, of the particle diameters are also given.

where B_0 is B_{c2} at $\theta = 0°$, θ the angle between the magnetic field and the YBCO c-axis and γ the anisotropy parameter. Often γ is extracted from the J_c data, but it is then denoted as γ_{eff} because of the extrinsic nature of J_c. It has been demonstrated that γ_{eff} can be changed by doping [9], but that the intrinsic γ is also then changed [1, 10]. However, contrary results for the behavior of γ exist too [2, 11], i.e. that the γ does not change with doping.

For this report, the angular dependences of B_{c2} and the irreversibility field, B_{irr}, were measured using a pulsed magnetic field for PLD-made YBCO thin films at BCO doping levels of 0, 2 and 8 wt.% (hereafter BCO-0, BCO-2 and BCO-8, respectively). In addition, the shape and size of the BCO particles were studied in detail by transmission electron microscopy. The data is used to further discuss the reason behind the change in B_{c2}.

2. Experimental details

Details of the film deposition on $SrTiO_3$ (1 0 0) substrates and the target preparation can be found in [1, 12]. The BCO-0 sample was also used in [1]. The selection of concentrations was based on our previous work [13], where the 2 wt.% and the 8 wt.% BCO-doped films had a different dependence of B_{c2} on temperature.

The critical temperature T_c and the critical current density J_c were measured in an out-of-plane magnetic field configuration (**B**||**c** where **c** is the longest lattice vector of YBCO) by an AC measurement option of the quantum design physical property measurement system (PPMS). The T_c was defined as the onset temperature of the in-phase component of AC magnetization. The structural properties and phase purity were measured by a Philips Xpert pro x-ray diffractometer (XRD) with a Schulz texture goniometer. To investigate the YBCO matrix and BCO particles in detail, the samples were further imaged using a JEOL 2200 FS transmission electron microscope (TEM) with double Cs correctors, operated at 200 keV. The wedging cross-sectional TEM specimens were prepared by a modified mechanical polishing method. From the attained TEM data, the size distributions of the BCO particles were analyzed using ImageJ software.

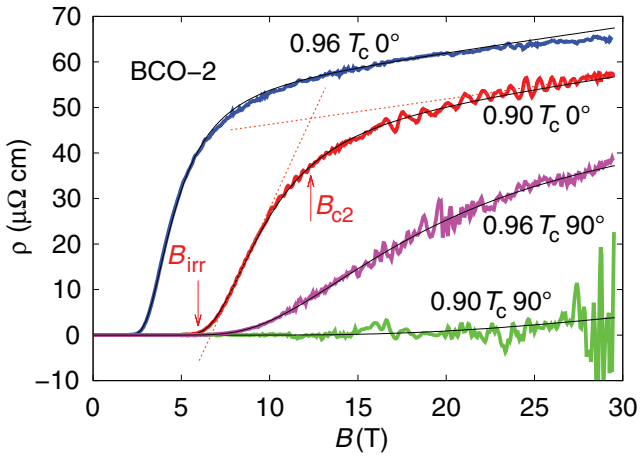

Figure 2. An example of the resistivity of the BCO-2 sample as a function of the magnetic field. The black solid line is a fit [1] used to phenomenologically describe the data. As an example, the tangents used to determine B_{c2} for $0.90T_c$ 0° are shown with dashed lines and B_{irr} and B_{c2} are indicated with arrows.

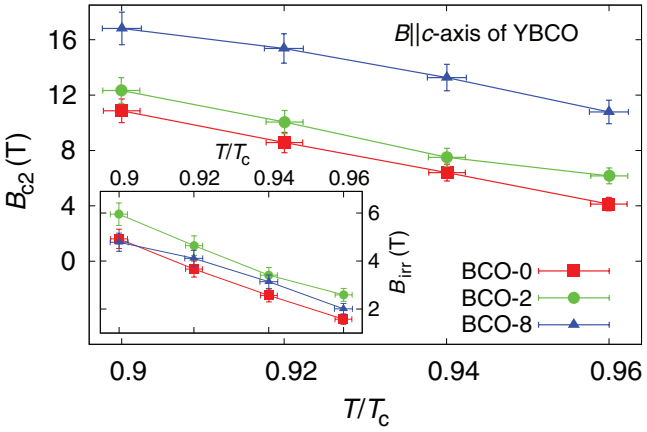

Figure 3. The upper critical field B_{c2} as a function of temperature T scaled with magnetic T_c in samples containing different amounts of BCO. The samples are oriented so that **B**||**c**. The temperature dependence of B_{irr} is shown in the inset.

To measure the critical fields, resistive measurements in pulsed magnetic fields up to 30 T with a pulse duration of 8 ms were carried out. The samples were first patterned into a 50 μm current stripe with a four-probe configuration using wet chemical etching. After that, the thicknesses of the films were determined by atomic force microscopy and the contacts on the samples were made by brazing them with indium. The samples were mounted in the maximum Lorentz force configuration on a rotating sample holder and measured in 10° steps from 0° to 100°, where the case 0° corresponds to **B**||**c**. The angles were calibrated in 1° steps by measuring the low-field resistivity with the sample in the superconducting transition and choosing the angle with the lowest resistivity to be 90°. The measurement temperatures were chosen to be $0.96T_c$ and $0.90T_c$ relative to the magnetically determined T_c. At angles 0° and 90°, measurements were also made at $0.92T_c$ and $0.94T_c$. All the measurements were made with a 200 μA current.

3. Results and discussion

The structural properties of the films, as measured by XRD, are similar to those measured before [7, 12]. As the BCO content increases, the full width at half maximum (FWHM) of the YBCO (0 0 5) reflection increases, indicating an increase in microstrain along [0 0 l]. In addition to the broadening, the peaks also shift to lower values of 2θ, indicating an increase in the length of the c-axis. This is in line with previous studies, where the introduction of a dopant lengthens the c-axis [7, 14, 15]. The rocking curve of YBCO (0 0 5) also broadens with a higher BCO concentration, implying an increase in out-of-plane splay.

Both BCO-2 and BCO-8 contain spherical BCO particles (figures 1(a) and (b)). Some of the particles are clustered into lines along the *ab*-planes of YBCO. Similar clustering has also been seen in PLD-made YBCO films containing Y_2O_3 particles [11]. At higher BCO concentrations the particles become more aggregative. The average diameter of the BCO particles (figures 1(c) and (d)) is 1.6 nm in BCO-2 whereas the particles in BCO-8 are 3.6 nm in diameter. In addition, the film with 4% BCO has a particle size of 2.5 nm [7], logically suggesting that the particle size tends to grow with BCO content. This is in contrast to BZO-doped YBCO, which creates an increased number of rods with the same diameter as the concentration of the dopant increases [16]. The size distribution of BCO-2 particles is skewed to the right, i.e. there is a greater number of larger particles than the average suggests. In contrast, the size distribution of BCO-8 is rather symmetric. In addition to distortions directly related to BCO, the samples also contain a large amount of stacking faults, which can be seen as line-type contrasts in the images.

The increase in BCO concentration also correlates to the superconducting properties. The critical temperatures measured from the magnetization data are $T_c = 87.6$ K and $T_c = 83.2$ K for BCO-2 and BCO-8, respectively. The T_c of the undoped reference BCO-0 sample is 88.6 K [1]. The behavior of T_c and J_c are in line with previously published results [7, 12], where both $J_c(0)$ and T_c decrease with an increasing BCO concentration, due to distortions created by the BCO. The addition of BCO also widens the transition: BCO-2 has $\Delta T_c = 1.4$ K, whereas BCO-8 has $\Delta T_c = 3.2$ K. On the other hand, the in-field values of J_c are enhanced by a moderate BCO addition [12]. At 10 K in the field of 3 T, the J_c is 7.3 MA cm^{-2} for the undoped sample, whereas the 2 and 4 wt.% BCO-doped samples have 8.9 MA cm^{-2} and 7.9 MA cm^{-2} [7], respectively.

The critical fields were extracted from the magnetic field dependences of resistivity. Examples of the resistivity of BCO-2 are shown in figure 2. The measured resistivity of a sample depends both on the temperature and orientation in the magnetic field. For the purposes of analysis, the data was fitted using a function consisting of an exponential function multiplied by a first degree polynomial [1, 17]. The B_{irr} was defined to be the field at which the fitted resistance was 1% of the normal state value. The B_{c2} was defined to be at the intersection of two tangents drawn at the steepest point of the transition and normal state resistance [1, 2].

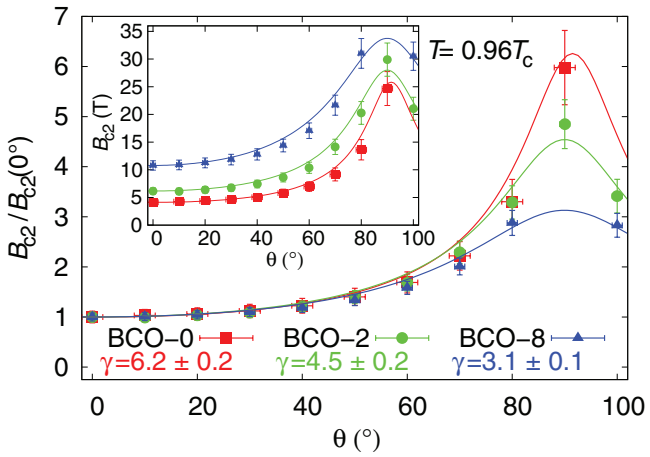

Figure 4. The angular dependence of B_{c2} at $T = 0.96T_c$ scaled with the **B**‖**c** values. The solid lines are fits to the Blatter scaling [1, 8]. The inset shows the absolute values of $B_{c2}(\theta)$ at $T = 0.96T_c$.

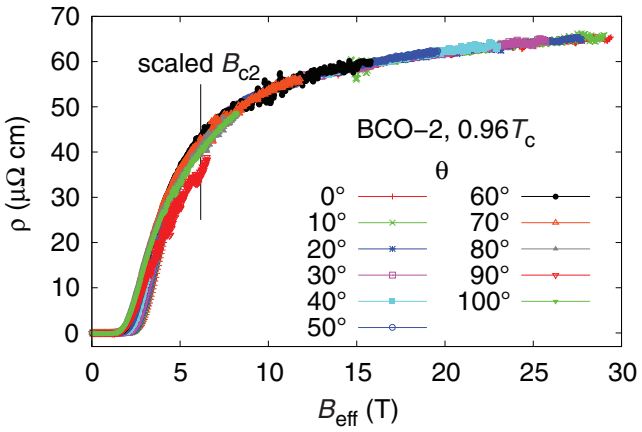

Figure 5. The resistivity of BCO-2 at $0.96T_c$ at different angles scaled using the effective magnetic field and the fitted γ.

The temperature dependence of B_{c2} at the angle $\theta = 0°$, i.e. when **B**‖**c**, is rather linear at all concentrations (figure 3) at the measured temperature range $0.90T_c$–$0.96T_c$. The larger the BCO concentration, the larger the B_{c2}. The error bars in the figure correspond to the sum of errors from the fitting of the phenomenological $\rho(B)$ equation and errors that are caused by uncertainties in the temperature and in the magnetic field. The errors were calculated by using the total differential of the magnetic field and assuming that all the errors have an affect at the same time. Additionally, calculating T_c by extrapolating the $B_{c2}(T)$ to $B_{c2} = 0$ yields the critical temperatures of 88.3 K [1], 88.9 K and 89.0 K for BCO-0, BCO-2 and BCO-8, respectively (called extrapolated T_c hereafter). The extrapolated T_c is higher than the magnetic T_c due to the percolative probing current that only needs a much smaller part to be superconducting compared to the detection limit of the magnetic measurement. Because the measurement temperatures were chosen relative to the magnetic T_c, BCO-8 was measured at a lower temperature than BCO-2 with regard to the extrapolated T_c. On the other hand, from the inset of figure 6, it can be seen that in a series of BCO concentration the magnetically determined T_c and T_c in the zero-field measured resistivity curves (called resistive T_c hereafter) correspond well to each other, with an approximately constant shift. Thus, we can conclude that the magnetic T_c can be used as a proxy for the zero-field resistive T_c. Additionally, the values of the B_{irr} are rather close to each other in different samples (figure 3 inset) and the values are roughly the same as in the BZO-doped samples [18]. The dependences of B_{irr} as a function of temperature are also rather linear at all concentrations.

The angular dependence of B_{c2} is clearly affected by the BCO concentration as well (figure 4 inset). The higher the content of BCO, the higher B_{c2} is through all angles. The relative change in B_{c2} with concentration is larger at $\theta = 0°$ (i.e. **B**‖**c**) than at $\theta = 90°$. The solid lines in figure 4 are fits to the Blatter scaling [1, 8]. They describe the data well at all angles. The fit has been done simultaneously for both temperatures, but since the $B_{c2}(\theta)$ values at $0.90T_c$, $\theta > 60°$ are above 30 T, and thus unreliable, they are omitted in the analysis.

There are no significant differences in the angular dependences of the B_{c2} between $0.90T_c$ and $0.96T_c$, but at $0.90T_c$ the highest values are above the measurement limit of 30 T. The data for $0.96T_c$ is shown in figure 4, scaled with the out-of-plane values and unscaled in the inset of figure 4. The data from BCO-0 gives a γ value of 6.2, whereas BCO-2 and BCO-8 can best be fitted with $\gamma = 4.5$ and 3.1, respectively.

As the scans of resistivity are plotted using the same scaling as in equation (1), we get the effective magnetic field, $B_{eff} = B[\cos^2(\theta) + \sin^2(\theta)/\gamma^2]^{1/2}$ (figure 5)—also used in [9, 19]. It can be seen that at around B_{c2} the curve collapses to a single line, whereas around B_{irr} there is a spread of curves depending on the angle between the magnetic field and the sample. The behavior of BCO-0 and BCO-8 is similar and thus not shown. The figures also show that for angles around $\theta = 90°$ a 30 T pulse is not enough to overcome the transition and the pulse does not necessarily reach B_{c2}. In these cases, the errors of the parameters of the fitted function also become rather large, as can be seen in figure 4.

The apparent effect of the BCO content on the values of B_{c2} may originate from the discrepancies between the extrapolated and magnetic T_c values. This, however, does not explain the change of γ, since it has been seen that below approximately $0.95T/T_c$, the values of γ are roughly constant [10, 11]. In other words, the differences in γ cannot be attributed to the uncertainty related to the definition of T_c.

Both the BCO- and BZO-doped samples [1] demonstrate changes in B_{c2} and γ compared to the undoped samples. Previously, the increase in B_{c2} was attributed to the scattering of electrons from the interface between the superconductor and the dopant, or to the strain caused by the dopant [10, 20]. Similar improvements in B_{c2} due to disorder have also been seen in Nb_3Sn [21], for example. In general, it has been seen that by adding non-magnetic impurities to a superconductor, the anisotropy becomes smaller and the T_c decreases [22, 23].

The improvement in B_{c2}, which is attributed to increased electron scattering, can be understood by considering the dirty limit of superconductors. According to the dirty limit Ginzburg–Landau model [24, 25], in cases of isotropic scattering, the γ

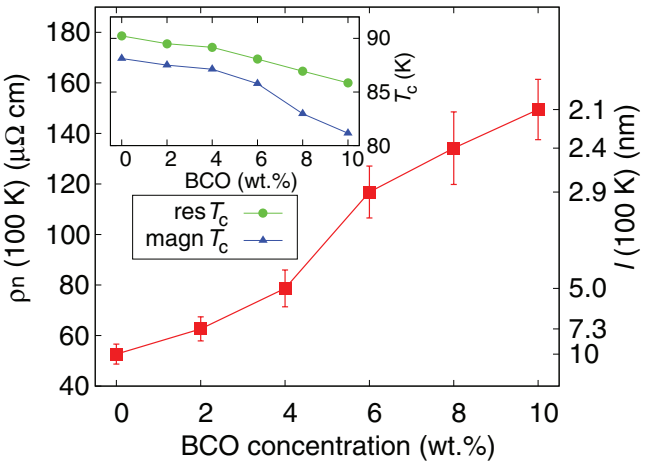

Figure 6. The normal state resistivity at 100 K as a function of BCO concentration as measured from our other BCO sample series. The estimated mean free path at the same temperature is shown on the right. The inset shows the critical temperatures of the same sample series measured both resistively in zero-field and magnetically.

in the anisotropy of B_{c2} (equation (1)) is replaced by the diffusivity ratio, which in turn depends on the mean free path [26]. When the coherence lengths are not restricted by the mean free path, the B_{c2} depends on γ and ξ as [27, p 361]

$$\gamma = \frac{B_{c2,ab}}{B_{c2,c}} = \frac{\xi_{ab}}{\xi_c}, \tag{2}$$

where $B_{c2,ab}$ ($B_{c2,c}$) is the B_{c2} when $\mathbf{B} \perp \mathbf{c}$ ($\mathbf{B} \| \mathbf{c}$). Assuming that the diffusivity can be estimated with the mean free path limited ξ as [28, p 410] $\xi_i^{-1} = \xi_{0,i}^{-1} + l^{-1}$, where i is either the direction of ab or c, ξ_0 the unrestricted coherence length and l the mean free path determined by the impurities, we can calculate the mean free paths from the apparent anisotropy of B_{c2} obtained from the above fits. Taking the coherence lengths at 0 K as $\xi_{0,ab} = 1.6$ nm and $\xi_{0,c} = 0.3$ nm [29] and the temperature dependence to be [27, p. 145, 148] $\xi \propto (1 - T/T_c)^{-1/2}$, we get $\xi_{0,ab} = 4.8$ nm and $\xi_{0,c} = 0.9$ nm for BCO-2 and $\xi_{0,ab} = 4.0$ nm and $\xi_{0,c} = 0.8$ nm for BCO-8 at $0.90T_c$. The impurity-restricted mean free path is $l = 20$ nm and $l = 3.8$ nm for BCO-2 and BCO-8, respectively.

In addition, a simple numerical mean free path calculation based on the uniform spatial distribution of BCO particles with the same size distributions and concentrations as in figure 1, gives a mean free path of about 31 nm for BCO-2 and 15 nm for BCO-8. The mean free path can also be estimated by using the normal state resistivity values. We observe a rise in the normal state resistivity ρ_n as a function of BCO concentration (figure 6). The resistivity of an undoped sample at 100 K is roughly 50 $\mu\Omega$ cm, whereas the 10 wt.% doped sample has a resistivity of 150 $\mu\Omega$ cm. The errors in the values are based on the uncertainty of the determination of the measurement stripe dimensions. The change in resistivity was converted into a change in the mean free path l (the right-hand scale in the figure 6) with the assumption that l for the undoped sample is the same as for a single crystal at 100 K, roughly 10 nm [30], and that the excess resistivity in the doped samples is purely due to the impurity scattering. Thus, the BCO additions clearly decrease the mean free path in the normal state. Because there are more defects in thin films than single crystals and the twin boundaries in thin films also restrict the mean free path remarkably [31], this overestimates the absolute value of l. The YBCO mean free path for a single crystal at around $0.90T_c$ is roughly 30 nm [30]. Using this value for the BCO-0, and assuming that the resistivity ratios are the same as at 100 K, we get the mean free path to be 22 nm and 7.3 nm for 2% BCO and 8% BCO, respectively. The mean free paths are very close to the values calculated by using the fitted γ.

The above-calculated values of l are smaller for the doped samples than for the undoped sample, indicating that the dopants do indeed shorten the mean free path. It is additionally shortened by strain and other defects created by BCO, which are especially seen in BCO-8. All these suggest that the shortening of the mean free path is responsible for the increase in the B_{c2}. Additionally, the coherence length ξ_c is intrinsically smaller than ξ_{ab} and thus the restricting effect of the uniformly distributed BCO particles is smaller in the $\mathbf{B} \perp \mathbf{c}$ direction. Therefore, the anisotropic change in B_{c2} leads to the decrease in γ. It is also noteworthy that the smallest γ is achieved at a much higher concentration than the highest value of $J_c(B)$.

This dirty limit explanation can equally well be used to explain the observed increase in B_{c2} on BZO- [1] and $BaHfO_3$-doped YBCO [20]. In contrast, in the cases of CSD-made YBCO with large BZO particles [2], there are no changes seen in γ because the large BZO particles are far away from each other and do not restrict the mean free path remarkably; thus, no changes in γ are seen.

4. Conclusions

To conclude, the angular dependences of B_{c2} in BCO-doped YBCO thin films were measured in pulsed magnetic fields up to 30 T. The introduced BCO distorts the YBCO structure but improves flux pinning by forming spherical particles whose diameter depends on the concentration of the dopant. Additionally, B_{c2} is increased by the doping. The relative change is largest in the case $\mathbf{B} \| \mathbf{c}$ and thus doping also lowers the intrinsic anisotropy. The mechanism behind the improvement is likely to be the scattering of electrons from the BCO-related defects, with the dopant causing the YBCO to be close to the dirty limit. The dirty limit can be used to explain the changes in B_{c2} in films with other dopants as well.

Acknowledgments

The Jenny and Antti Wihuri Foundation and the Finnish Cultural Foundation are acknowledged for their financial support. This work made use of the Aalto University Nanomicroscopy Center (Aalto-NMC) facilities.

References

[1] Palonen H, Huhtinen H, Shakhov M A and Paturi P 2013 *Supercond. Sci. Technol.* **26** 045003
[2] Llordés A *et al* 2012 *Nat. Mater.* **11** 329–36
[3] Yamada H, Yamasaki H, Develos-Bagarinao K, Nakagawa Y, Mawatari Y, Nie J C, Obara H and Kosaka S 2004 *Supercond. Sci. Technol.* **17** S25–9
[4] Goyal A *et al* 2005 *Supercond. Sci. Technol.* **18** 1533–8
[5] Malmivirta M, Yao L, Huhtinen H, Palonen H, van Dijken S and Paturi P 2014 *Thin Solid Films* **562** 554–60
[6] Gutiérrez J *et al* 2007 *Nat. Mater.* **6** 367–73
[7] Malmivirta M, Yao L D, Inkinen S, Huhtinen H, Palonen H, Jha R, Awana V P S, van Dijken S and Paturi P 2015 *IEEE Trans. Appl. Supercond.* **25** 6603305
[8] Blatter G, Feigel'man M V, Geshkenbein V B, Larkin A I and Vinokur V M 1994 *Rev. Mod. Phys.* **66** 1125–388
[9] Paturi P, Irjala M and Huhtinen H 2008 *J. Appl. Phys.* **103** 123907
[10] Miura M, Baily S A, Maiorov B, Civale L, Willis J O, Marken K, Izumi T, Tanabe K and Shiohara Y 2010 *Appl. Phys. Lett.* **96** 072506
[11] Xu A, Jaroszynski J, Kametani F and Larbalestier D 2015 *Appl. Phys. Lett.* **106** 052603
[12] Irjala M, Huhtinen H, Jha R, Awana V P S and Paturi P 2011 *IEEE Trans. Appl. Supercond.* **21** 2762–6
[13] Huhtinen H, Palonen H, Malmivirta M, Jha R, Awana V P S and Paturi P 2014 *J. Phys. Conf. Ser.* **507** 012020
[14] Huhtinen H, Irjala M, Paturi P and Falter M 2010 *IEEE Trans. Appl. Supercond.* **21** 2753–7
[15] Sieger M *et al* 2015 *IEEE Trans. Appl. Supercond.* **25** 6602604
[16] Peurla M, Paturi P, Stepanov Y P, Huhtinen H, Tse Y Y, Bódi A C, Raittila J and Laiho R 2006 *Supercond. Sci. Technol.* **19** 767–71
[17] Peurla M, Huhtinen H, Shakhov M A, Traito K, Stepanov Y P, Safonchik M, Paturi P, Tse Y Y, Palai R and Laiho R 2007 *Phys. Rev.* B **75** 184524
[18] Huhtinen H, Irjala M, Paturi P, Shakhov M A and Laiho R 2010 *J. Appl. Phys.* **107** 053906
[19] Sarti S, Giura M, Silva E, Fastampa R and Boffa V 1997 *Phys. Rev.* B **55** R6133–6
[20] Matsushita T *et al* 2012 *Supercond. Sci. Technol.* **25** 125003
[21] Cooley L D, Hu Y F and Moodenbaugh A R 2006 *Appl. Phys. Lett.* **88** 142506
[22] Clem J R 1967 *Phys. Rev.* **153** 449–54
[23] Anderson P W 1959 *J. Phys. Chem. Solids* **11** 26–30
[24] Golubov A A and Koshelev A E 2003 *Phys. Rev.* B **68** 104503
[25] Gurevich A 2003 *Phys. Rev.* B **67** 184515
[26] Kim H J, Lee H S, Kang B, Yim W H, Jo Y, Jung M H and Lee S I 2006 *Phys. Rev.* B **73** 064520
[27] Poole C P Jr, Farach H A, Creswick R J and Prozorov R 2007 *Superconductivity* 2nd edn (New York: Academic)
[28] Bleaney B I and Bleaney B 1976 *Electricity and Magnetism* (Oxford: Oxford Science Publications)
[29] Welp U, Kwok W K, Crabtree G W, Vandervoort K G and Liu J Z 1989 *Phys. Rev. Lett.* **62** 1908–11
[30] Krishana K, Harris J M and Ong N P 1995 *Phys. Rev. Lett.* **75** 3529–32
[31] Jacobs T, Numssen K, Schwab R, Heidinger R and Halbritter J 1997 *IEEE Trans. Appl. Supercond.* **7** 1917–20